

Design and Optimization of He-Xe Brayton cycles system for MW-level space nuclear reactor application*

Yun-Cheng Gao,^{1,2} Si-Miao Tang,^{1,2,†} Lu-Teng Zhang,^{1,2} and Liang-Ming Pan^{1,2}

¹*Key Laboratory of Low-grade Energy Utilization Technologies and Systems,
Ministry of Education, Chongqing University, Chongqing 400044, China.*

²*Department of Nuclear Engineering and Technology, Chongqing University, Chongqing 400044, China.*

Space reactor power has a good future in sea, land, air and space by virtue of its small size, applicability and high efficiency, and the combination of high temperature gas-cooled reactor and Brayton cycle is more suitable for exploration missions at the megawatt power level. A space gas-cooled reactor with a thermal power of 3 MW is used as a research object, and the design and optimization of this research object is carried out using EBSILON simulation software. The efficiency comparison between direct and indirect Brayton cycle is carried out under different conditions, the direct Brayton cycle was found to be 1.4%-2.8% more efficient than the indirect Brayton cycle and occupies less space. The efficiencies of four configurations of the Brayton cycle are compared. When the compressor inlet temperature is 400 K, the recompression efficiency is lower, and the efficiency of both the interstage-cooled cycle and the simple reheat cycle is higher than 30% when the turbine inlet temperature reaches 1400K. When the compressor inlet temperature is 350K, the simple reheat cycle can achieve 29.6% efficiency at a turbine inlet temperature of 1200K. When the compressor inlet temperature is 300K, the efficiency of all four cycle structures is higher than 20%. And when the turbine inlet temperature is higher than 1150K, the efficiency of all four structures is higher than 30%. The optimal pressure ratios are different for the different configurations, with 2.2 and 3.5 for the simple reheat cycle and the interstage-cooled cycle, respectively. And the optimal pressure ratio for the recompression cycle is also related to its diversion ratio, the recompression cycle efficiencies are 0.417 and 0.141 when the splitting ratios are 0 and 0.4, respectively. In actual operation, the pressure loss of the system is unavoidable. It is found that the efficiency reduction caused by the high pressure relative loss is 1.7% higher than the reduction caused by the low pressure relative loss. In addition, the recuperator effectiveness and the efficiency of the TAC also affect the system cycle efficiency to some extent. The exergy analysis method was also used to verify that the recompression cycle efficiency was lower than the simple reheat cycle efficiency. The losses in both are concentrated in the cooler and reactor, with the cooler and reactor losses of the recompression cycle together accounting for 79.6% of the total losses. Finally, the simple reheat cycle was taken as the optimal structure, and a space reactor system with a thermal power of 3 MW and an electrical power of 1 MW is successfully designed.

Keywords: Brayton cycle; Space nuclear reactor; Exergy analysis method; Design and optimization

I. INTRODUCTION

Energy is indispensable to industry, military and people's livelihood. And with the advancement of science and technology, mankind is now gradually strengthening its exploration of the sea, land, air and sky. However, solar energy is not an autonomous energy source, the mission cycle of chemical energy is short, and the power level of radioisotope nuclear power source is low. So for high-power level mission, the above energy sources can hardly be used[1]. The new mobile reactor system does not depend on sunlight and has high energy density, which has been widely studied and applied in the field of sea, land, air and space[2]. For the main technical aspects of the space reactor system, it is necessary to consider three aspects: firstly, the safety and economy of the reactor power supply. Secondly, the performance of the reactor power supply, which is aim to improve the power to mass ratio of the reactor power supply as much as possible. And lastly, the applicability of the reactor power supply.

Based on the excellent characteristics of the new portable reactor system, as early as a few decades ago, some scholars in the world have done a lot of research on the space reactor power supply. In 2003, the United States NASA(National Aeronautics and Space Administration) set up a project "Prometheus" program, the main goal is to develop a high-power space nuclear reactor power supply. In 2009, Russia began to develop the MWe-class nuclear propulsion spacecraft[3], which consists of an ultrahigh-temperature gas-cooled reactor and a Brayton cycle system, and it guides for the design and development of subsequent space reactors. ESA(European Space Agency) is also working on the "Prometheus" program. ESA is also vigorously developing space nuclear power technology, mainly through the implementation of the DiPoP(Disruptive Technologies for Power and Propulsion)[4] project and the MEGAHIT[5] program, and has completed the technical selection of various systems of nuclear electric propulsion.

Based on the exploratory experience of the previous researchers, more and more researches on the space reactors have appeared. Ju et al.[6] proposed a conceptual design scheme for a helium-xenon gas-cooled fast reactor consisting of hexagonal prismatic fuel elements, and also investigated the thermo-hydraulic characteristics of the reactor. Yang et al.[7] also presented the neutron physical analysis on a pris-

* This work is Funded by Natural Science Foundation of Chongqing, China2023NSCQ-BHX0243.

† Corresponding author, Si-Miao Tang, complete address:simiao_tang@cqu.edu.cn, telephone number:+86 18829581798.

matic space gas-cooled reactor. Jiang et al.[8] developed a simple mass estimation model based on a preliminary optimized shielding design for the Jupiter Icy Moon Orbiter (JIMO) reactor. Yue et al.[9] studied OMEGA (Open-grid Megawatt Gas-cooled spAce nuclear reactor) and also developed TASS (Transient Analysis code of scheduled Shutdown and emergency Shutdown). Based on this, it was also concluded that surface coatings on the fuel cladding can greatly improve radiative heat transfer. Qin et al.[10] conducted an optimization analysis of the energy conversion efficiency and radiator mass of an air-cooled space nuclear reactor and investigated the performance of HPR (heat pipe radiator) and LPR (liquid droplet radiator), respectively. Meng et al.[11] performed numerical simulations of a 1/12 full-core air-cooled space nuclear reactor using the STAR- CCM + program and a series of calculations of a complex core structure under zero-gravity conditions. Li et al.[12] proposed a conceptual design for an integrated space air-cooled reactor based on TRISO fuel with an electrical power output of 200 kW. It was finally concluded that helium-xenon mixture is the optimal work mass. Alfonso Biondi et al.[13] modeled and simulated a closed Brayton cycle system driven by a solar parabolic collector, which improved the efficiency by 7.4%, reduced the weight by 21%, and achieved a specific mass of the system of 30 kg/kW. Guilherme B. Ribeiro et al.[14] developed a closed regenerative Brayton cycle model which is used to calculate the size of the heat exchangers in the system. And the mass of the heat exchangers in the space reactor is also optimized. Wu et al.[15] examined the transient response safety of gas-cooled reactors and investigated the performance of the overall system of coupled Brayton cycles using a self-developed thermal-hydraulic system analysis program.

He-Xe gas mixtures are often used in reactors on land, sea, air and space. Thanks to the support from the fields of chemistry and gas dynamics, there are many studies on the nuclear aspects of He-Xe gases. Wang et al.[16] optimized a model for the calculation of the physical properties of He-Xe gas mixtures, and obtained a systematic property analysis procedure suitable for the calculation of the natural circulation of He-Xe gas mixtures. Adil Malik et al.[17] analyzed the advantages of using helium-xenon over pure helium in the turbocompressor of a high-temperature gas-cooled reactor (HTGR) power plant. Ma et al.[18] established a link between the thermodynamic performance of a megawatt-scale space reactor system and its mass, and investigated the effects of different binary mixtures of noble gases on the performance and mass of the system. It was finally concluded that helium-xenon mixture is the optimal mass. Wang et al.[19] numerically investigated the thermo-hydrodynamic properties of the He-Xe gas mixture inside a 2×2 helix wrapped rod bundle, which provides a basis for the thermo-hydrodynamic design of He-Xe gas-cooled space nuclear reactors.

The combination of high-temperature gas-cooled reactors (HTGR) and Brayton cycle systems is an important research object for space reactor power supply[20, 21]. Most of the current studies mainly focus on two aspects: the core design of high-temperature gas-cooled reactors and the design optimization of the components in the Brayton cycle, but there

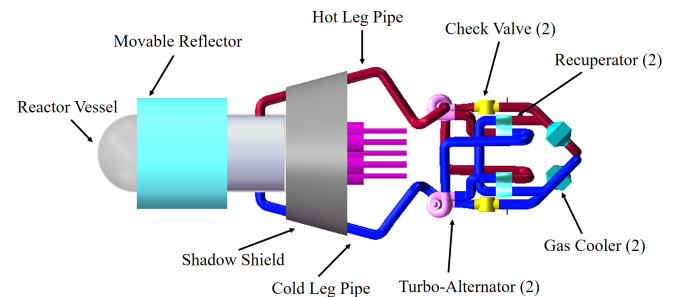


Fig. 1. The cross-section of the gas-cooled reactor coupled Brayton cycle system

are fewer studies on the structural selection of the Brayton cycle. For common gases such as air and supercritical CO₂, the structure of different Brayton cycles will have a large impact on the cycle efficiency. As for the He-Xe gas mixture with large adiabatic index, the optimal Brayton cycle structure and the optimal cycle parameters will be sought in this paper on the basis.

II. INTRODUCTION TO THE SYSTEM AND MODEL

A. High Temperature Gas-Cooled Reactor (HTGR) Model

1. High Temperature Gas-Cooled Reactor (HTGR) Model

The high-temperature gas-cooled reactor used in this paper is an open-grid high-temperature gas-cooled reactor[22], which mainly consists of upper and lower grids, 654 fuel elements and 13 control rods. The upper and lower grids are used for axial positioning of the fuel elements, and the cylindrical fuel elements are arranged in a triangular shape in the core with a spacing of 14.2 mm. The control rods have a B4C core block inside and a 1-mm-thick shell outside, with a gap in the middle made of metal rubber to compensate for the radial deformation caused by fission gases, etc. A schematic diagram of a high-temperature gas-cooled reactor coupled to a Brayton cycle is shown in Fig 1.

The fuel element consists mainly of the uranium dioxide fuel pellet, the hot-end and cold-end reflector layers, the casing and the liner. The core block is a sintered disc of uranium dioxide fuel with an internal center hole, the cladding is made of Mo-Nb-Zr alloy. The center hole serves to vent the gaseous fission products into the gas replenishment space of the fuel element with the help of a dedicated venting device. Table 1 lists the design parameters of the open-grid HTGR:

B. Brayton Cycle Model

The Brayton cycle is a reliable thermal cycle, it has been widely used in many fields by virtue of its efficiency and applicability. A simple Brayton cycle consists of four main processes: Adiabatic compression, isobaric heating, adiabatic

Parameter	Value	Parameter	Value
Neutron energy spectrum	fast reactor	Thickness of radial reflective layer/cm	10.3
Reactor power/MWt	3.4	Number of fuel rods	732
Coolant flow/kg · s ⁻¹	14.236	Number of control rods	13
Control rod conduit outer diameter/cm	3.5	Fuel rod spacing/cm	1.41
Core diameter/cm	41.6	UO ₂ Fuel core block inner diameter/mm	3.0
Inner diameter of descending section/cm	44.4	UO ₂ Fuel core block outer diameter/mm	10.9
Outer diameter of descending section/cm	46.4	Air gap thickness/mm	0.05
Pressure vessel thickness/cm	0.6	Shell thickness/mm	1.0
Pressure vessel outer diameter/cm	47.6	Fuel area height/cm	55.0

Table 1. Design parameters for open-grid HTGR

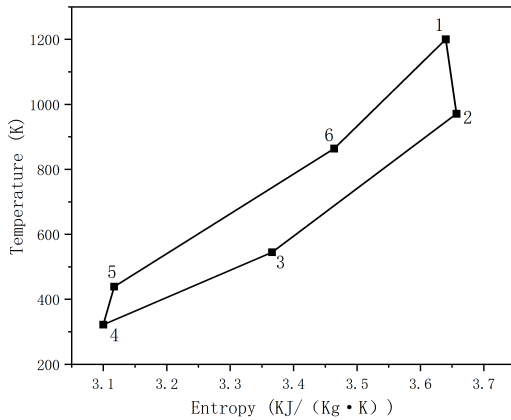


Fig. 2. Temperature-entropy diagram for simple reheat Brayton cycle

expansion and isobaric exotherm. The core of the Brayton cycle is the TAC, which consists of a turbine, compressor and generator arranged on the same rotor shaft. The work of the turbine is distributed to the compressor and generator through the rotor shaft, allowing the Brayton cycle to operate. In addition to this, there are coolers, recuperators and other components in the space reactor.

The temperature-entropy diagram of a simple reheat Brayton cycle is shown in Fig. 2. First, the high-temperature He-Xe gas mixture from the gas-cooled reactor outlet enters the turbine to do work (1-2). At this point, the high-temperature He-Xe gas mixture enters the recuperator and transfers heat to the other side of the recuperator (2-3). It then enters the external cooler where it is cooled by NaK on the tube side (3-4). The cooler fluid enters the compressor (4-5) and the excess work is used to generate electricity. The fluid then enters the recuperator to be heated by the fluid on the other side (5-6) and finally flows back into the core to be heated to the required turbine inlet temperature (6-1).

In order to maximize the heat utilization, a recompressor is added to the recompression cycle while splitting the recu-

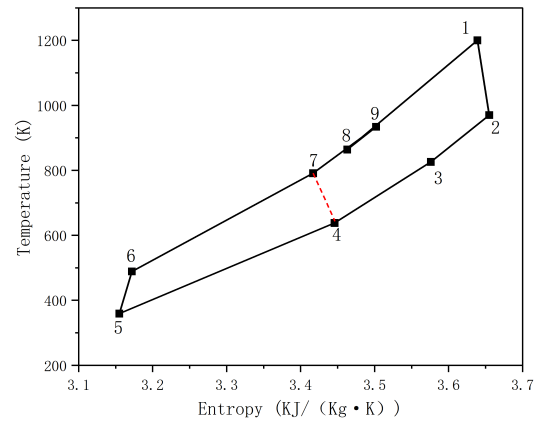


Fig. 3. Temperature-entropy diagram for recompression cycle

perator into two. The temperature-entropy diagram of the recompression cycle is shown in Fig 3. Unlike the simple reheat Brayton cycle, the fluid flowing from the low-temperature recuperator is split in two through a splitter, and then enters the main compressor and the recompressor (4-5-6 and 4-7). The fluid passing through the recompressor meets another portion of the fluid heated by the high-temperature recuperator (7-8), and it is finally heated by the low-temperature recuperator and core. This configuration increases the enthalpy at the core inlet, thereby increasing the cycle efficiency for some fluid.

The compressor is the main power-consuming component in the Brayton cycle, and reducing its power consumption can improve the efficiency of the system cycle. The power consumption is related to the compressor inlet temperature. The interstage-cooled cycle divides the compressor into two, and a cooler is added between two compressors, so that the inlet temperature of the second compressor can be reduced. Thus the total power consumption is reduced. The diagram of the interstage cooling cycle is shown in Fig.4.

C. Turbomachinery model

1) Power balance

The power of the TAC shaft is equal to the power produced by the turbine minus the power consumed by the compressor and generator. This TAC model combines the rotor shaft power with the rotational speed. When the rotor shaft power is positive, the faster the rotor shaft will rotate, and the slower the rotor shaft will rotate when the shaft power is negative. The mathematical expression is given as:

$$\frac{dN_{Shaft}}{dt} = \frac{P_{Shaft}}{I \cdot N_{Shaft} \cdot 4\pi^2} \quad (1)$$

Power balance equation on the rotating shaft:

$$P_{Shaft} = P_{Tur} - P_{Com} - P_{Alt} \quad (2)$$

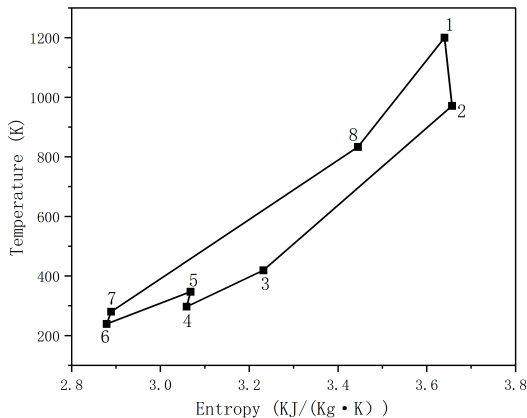


Fig. 4. Temperature-entropy diagram for interstage-cooled cycle

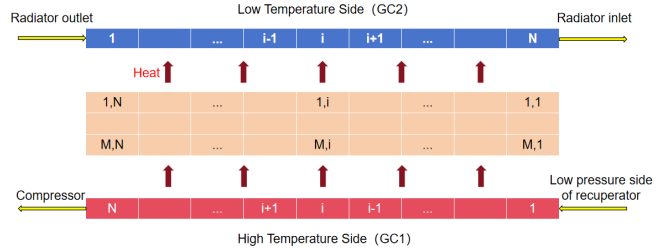


Fig. 5. Schematic diagram of the control volume division of the heat exchanger model

Where: P_{cout} —Compressor outlet pressure/Pa; P_{cin} —Compressor inlet pressure/Pa; f_{PrC} —Equation of the pressure-ratio characteristic curve of the compressor; f_{TrC} —Equation for the compressor temperature-ratio characteristic curve; P_{tout} —Turbine outlet pressure/Pa; P_{tin} —Turbine inlet pressure/Pa; f_{PrT} —Turbine pressure-ratio characteristic curve equation; f_{TrT} —Turbine temperature ratio characteristic curve equation.

190 Power generated by the turbine:

$$P_{Tur} = W_{Tur} \cdot C_{p,g}(T_{cin} - T_{cout}) \quad (3)$$

192 Power consumed by the compressor:

$$P_{Com} = W_{Com} \cdot C_{p,g}(T_{cin} - T_{cout}) \quad (4)$$

194 Where: N_{Shaft} —TAC rotating shaft speed/s⁻¹; P_{Shaft} —
195 TAC rotor shaft power/W; I —Rotor shaft moment of
196 inertia/kg · s². P_{Tur} —Turbine power/W; P_{Com} —Compressor
197 power; P_{Alt} —AC Generator power/W; T_{tin} —Turbine inlet
198 temperature/K; T_{tout} —Turbine outlet temperature/K; T_{cin} —
199 Compressor inlet temperature/K; T_{cout} —Compressor outlet
200 temperature/K.

2) Flow Characteristic Curve

202 The work of the turbine and compressor is related to the
203 flow mass flow rate, inlet and outlet temperatures, which can
204 be obtained from the characteristic curve[23]. The flow char-
205 acteristic curve takes the temperature ratio and pressure ratio
206 as a function of inlet temperature, inlet pressure, mass flow
207 rate and shaft speed, which can be calculated given certain
208 boundary conditions.

209 Pressure ratio curve of a compressor:

$$\frac{P_{cout}}{P_{cin}} = f_{PrC}(T_{cin}, P_{cin}, W_{Com}, N_{Shaft}) \quad (5)$$

211 Temperature-ratio curves for pressurized gas engines:

$$\frac{T_{cout}}{T_{cin}} = f_{TrC}(T_{cin}, P_{cin}, W_{Com}, N_{Shaft}) \quad (6)$$

213 Pressure ratio curve of the turbine:

$$\frac{P_{tout}}{P_{tin}} = f_{PrT}(T_{tin}, P_{tin}, W_{Com}, N_{Shaft}) \quad (7)$$

215 Temperature-ratio curve of the turbine:

$$\frac{T_{tout}}{T_{tin}} = f_{TrT}(T_{tin}, P_{tin}, W_{Com}, N_{Shaft}) \quad (8)$$

D. Heat transfer model

226 There is at least one gas cooled in every space reactor Bray-
227 ton cycle, also known as an external cooler. It is an external
228 cold source to cool the Brayton cycle flow mass. It is a shell-
229 and-tube counter-current heat exchanger with fins, where the
230 high-temperature He-Xe gas is on the shell side and water
231 or liquid NaK flows on the tube side as the cooling medium.
232 The heat absorbed on the tube side is transferred to the space
233 through radiant heat dissipation, thus realizing a continuous
234 discharge of waste heat. Inside the cooler, there are 400 heat
235 exchanger tubes with an outer diameter of 6.35 mm, a tube
236 length of 2 m, and a wall thickness of 1.058 mm. Including
237 the fins, the effective gas-side heat exchanger area is 47 m².
238 The gas cooler model includes the heat exchanger model for
239 the flow of the fluids on the high and low temperature sides,
240 and the heat conductivity model for the heat exchanger tubes.

241 The model of the gas cooler includes the flow heat transfer
242 model of the fluid on both sides of the high and low tempera-
243 tures and the heat conduction model of the heat transfer tube.
244 The two-side flow heat transfer model calculates the pressure
245 and enthalpy of the fluid, and the wall heat conduction model
246 calculates the temperature of the heat exchanger tube, ignor-
247 ing the axial heat conduction of the heat exchanger tube wall
248 and assuming that the heat is transferred only in the radial di-
249 rection. The control volume of the model is divided as shown

250 in the Fig 5. First, the high and low temperature side and the
251 heat exchanger tube are divided into N control volumes, and
252 then the heat exchanger tube is divided into N control vol-
253 umes in the radial direction. Since the heat exchanger is a
254 counter-flow heat exchanger, it should be noted that the num-
255 bering order of the high temperature side and the low tem-
256 perature side should be reversed.

257 Energy conservation equation for the ith control volume of

the gas on the high temperature side:

$$\rho_{GC1}^i c_{p,GC1}^i \frac{dT_{GC1}^i}{dt} = W_{GC1in}(h_{GC1}^{i-1} - h_{GC1}^i) + l_i \prod_{GC1}^i H_{GC1}^i (T_{wall}^{M+2,i} - T_{GC1}^i) \quad (9)$$

$$= \frac{W_{GC1in}(h_{GC1}^{i-1} - h_{GC1}^i) + l_i \prod_{GC1}^i H_{GC1}^i (T_{wall}^{M+2,i} - T_{GC1}^i)}{l_i A_{GC1}} \quad (10)$$

Energy conservation equations for the i th control volume of the cooled mass on the low-temperature side:

$$\rho_{GC2}^i c_{p,GC2}^i \frac{dT_{GC2}^i}{dt} = [W_{GC2in}(h_{GC1}^{i-1} - h_{GC1}^i) + N_{pipe} l_i C_{tubeI} H_{GC2}^i] \quad (11)$$

$$= [W_{GC2in}(h_{GC1}^{i-1} - h_{GC1}^i) + N_{pipe} l_i C_{tubeI} H_{GC2}^i] \quad (12)$$

$$(T_{wall}^{1,N-i+3} - T_{GC2}^i)] / [N_{pipe} \cdot l_i A_{GC2}] \quad (13)$$

Thermal conductivity equation for the (j,i) th control volume of the intermediate heat exchanger wall:

$$N_{pipe} \cdot \rho_w^{j,i} c_{p,w}^{j,i} \frac{dT_w^{j,i}}{A_w^{j,i}} = \frac{\prod_{wI}^{j,i} (\frac{\lambda_w^{j-1,i} + \lambda_w^{j,i}}{2}) (\frac{T_w^{j-1,i} - T_w^{j,i}}{r_w^j - r_w^{j-1}})}{A_w^{j,i}} + \frac{\prod_{wO}^{j,i} (\frac{\lambda_w^{j+1,i} + \lambda_w^{j,i}}{2}) (\frac{T_w^{j+1,i} - T_w^{j,i}}{r_w^{m+1} - r_w^m})} \quad (14)$$

Boundary conditions on the inner surface of the heat exchanger tube:

$$(\frac{\lambda_w^{1,i} + \lambda_w^{2,i}}{2}) \frac{T_w^{2,i} - T_w^{1,i}}{r_w^2 - r_w^1} = H_{GC2}^i (T_w^{1,i} - T_{GC2}^{N-i+3}) \quad (17)$$

Boundary conditions on the outer surface of the heat exchanger:

$$(\frac{\lambda_w^{M+2,i} + \lambda_w^{M+1,i}}{2}) \frac{T_w^{M+2,i} - T_w^{M+1,i}}{r_w^{M+2} - r_w^{M+1}} = H_{GC1}^i (T_{GC1}^i - T_w^{M+2,i}) \quad (18)$$

Where: \prod –Channel heating perimeter/m; H –Convective heat transfer coefficient of the mass/ $W \cdot m^{-2} \cdot K^{-1}$; T_w –Heat exchanger tube wall temperature/K; W_{in} –Inlet mass flow rate/ $kg \cdot s^{-1}$; N_{pipe} –Number of heat exchanger tubes; C_{tubeI} –Heat exchanger tube inner circumference/m; W_{wallI} –Heat exchanger tube control volume inner surface circumference/m; W_{wallO} –Heat exchanger tube control volume outer surface circumference/m; Superscript i –Axial control volume number; Superscript j –Radial control volume number of the heat exchanger tube wall; Subscript GC1–High temperature side; Subscript GC2–Low temperature side; Subscript w–Heat exchanger tube wall.

In addition, in order to improve the utilization of heat and the thermal efficiency of the system, there is at least one plate-fin type recuperator in each Brayton cycle loop. The high-temperature fluid from the turbine outlet transfers the heat to the compressor outlet fluid at the later stage of the cycle, thus

realizing the preheating of the work mass. It can increase the enthalpy value of the point to a certain extent and reduce the heat absorbed by the work mass from the heap, so as to make a large improvement in the thermal efficiency of the cycle.

The basic model of the recuperator and the gas cooler is the same, and the difference between the two lies in the difference between the high and low temperature side of the work mass.

E. Auxiliary model

He-Xe gas mixtures have an important place in the field of space reactor research, and the combination of a Brayton cycle with a high-temperature gas-cooled reactor using He-Xe gas mixtures as the work mass is well suited for space reactor missions in the MW power missions. For the Brayton cycle circuit, the gas modeling is particularly important. In addition to this, the pressure loss and thermophysical properties of the mass in the pipeline have a significant impact on key parameters such as cycle efficiency.

For the transport properties of He and Xe single gases can be calculated by Chapman-Enskog theory, and then the properties of the two can be mixed by the method proposed by

Hirschfeld[24], which leads to the properties of He-Xe gas mixture. Since the molecular mass of both M_w , mole fraction x and adiabatic index γ are known, the average molecular mass of the gas mixture M_{w0} and the average adiabatic index γ_0 respectively:

$$M_{w0} = x_{Xe} + (1 - x_{Xe}) M_{He} \quad (19)$$

$$\gamma_0 = x_{Xe} \gamma_{Xe} + (1 - x_{Xe}) \gamma_{He} \quad (20)$$

The gas constant of the gas mixture is:

$$R_0 = R_g / M_{w0} \quad (21)$$

Where: $R_0=8.3145 \text{ J/(mol K)}$ is the ideal gas constant. Thus, the density ρ , speed of sound c and specific constant pressure heat capacity of the gas mixture c_p can be calculated by the following equation:

$$\rho(T, p) = p / R_0 T \quad (22)$$

$$c(T) = (\gamma R_0 T)^{1/2} \quad (23)$$

$$c_p(\gamma, M_w) = R_0 / M_{w0} (1 - 1/\gamma) \quad (24)$$

For the calculation of the kinetic viscosity μ and thermal conductivity λ , the Lennard-Jones potential theory is used in Hirschfeld's method, and the Lennard-Jones coefficients for He and Xe are, respectively:

$$\epsilon_{He} = 10.2K, \sigma_{He} = 2.576 \quad (25)$$

$$\epsilon_{Xe} = 229K, \sigma_{Xe} = 4.055 \quad (26)$$

340 The above coefficients combined with the transport theory
 341 prediction curve $\Omega(T)$ The equations for the calculation of the
 342 kinetic viscosity μ and thermal conductivity λ of monatomic
 343 gases can be obtained.

$$345 \quad \Omega(T) = 0.92495 + 2.07368 \times 10^{-3} T + 0.719288 T^{-1.151049} - 5.46452 \times 10^{-2} T^{1/2} \quad (27)$$

$$346 \quad \mu(M_w, \epsilon, \sigma, T) = (M_w T)^{1/2} / \sigma^2 \Omega(T/\epsilon) \times 2.6693 \times 10^{-6} \quad (28)$$

$$348 \quad \lambda(M_w, \epsilon, \sigma, T) = 8.322 \times 10^{-2} W/m \cdot (T/M_w)^{1/2} / \sigma^2 \Omega(T/\epsilon) \quad (29)$$

349 The transportation characteristics of the gas mixture can be
 350 determined by the following equation:

$$351 \quad \Phi_{HX}(T) = \frac{1}{\sqrt{8}} \left(1 + \frac{M_{wHe}}{M_{wXe}}\right)^{-0.5} \cdot \left[1 + \left(\frac{\mu_{He}(T)}{\mu_{Xe}(T)}\right)^{0.5} \left(\frac{M_{wXe}}{M_{wHe}}\right)^{0.25}\right]^2 \quad (30)$$

$$353 \quad \Phi_{HX}(T) = \frac{1}{\sqrt{8}} \left(1 + \frac{M_{wXe}}{M_{wHe}}\right)^{-0.5} \cdot \left[1 + \left(\frac{\mu_{Xe}(T)}{\mu_{He}(T)}\right)^{0.5} \left(\frac{M_{wHe}}{M_{wXe}}\right)^{0.25}\right]^2 \quad (31)$$

$$355 \quad \lambda_{mix}(T) = \frac{x_{He}\lambda_{He}(T)}{x_{He} + x_{Xe}\Phi_{HX}(T)} + \frac{x_{Xe}\lambda_{Xe}(T)}{x_{Xe} + x_{He}\Phi_{HX}(T)} \quad (32)$$

$$357 \quad \mu_{mix}(T) = \frac{x_{He}\mu_{He}(T)}{x_{He} + x_{Xe}\Phi_{HX}(T)} + \frac{x_{Xe}\mu_{Xe}(T)}{x_{Xe} + x_{He}\Phi_{HX}(T)} \quad (33)$$

358 F. Model verification

359 EBSILON is a power plant general visualization grouping
 360 thermodynamic mechanism modeling and heat balance cal-
 361 culation simulation software. The reactor is modeled using
 362 EBSILON to verify the reliability of EBSILON for the sim-
 363 ulation of space reactor, and the relevant parameters of the
 364 reactor are referenced in the literature[25]. The simulation
 365 results are shown in Table 2:

366 Compared to the reference values in the literature, the com-
 367 putational aberrations simulated by EBSILON are within the
 368 allowable deviation range. So they are therefore sufficient
 369 to demonstrate the reliable status of EBSILON in the simula-
 370 tion of space reactor power supply simulations for subsequent
 372 analysis.

373 III. RESULT AND DISCUSSION

374 A. Comparison of direct and indirect Brayton cycle 375 efficiencies

376 The direct Brayton cycle and the indirect Brayton cycle
 377 have their own advantages and disadvantages in research ap-
 378 plications. The direct Brayton cycle is compact and less ex-
 379 pensive, but the radioactivity will fill the entire Brayton cy-
 380 cle loop. The indirect Brayton cycle is able to physically
 381 separate the primary and secondary loops, thus isolating the

Parameter	EBSILON calculated value	Literature design value	Aberration	Modelica Language Calculated Values	Aberration
Reactor flow /kg · s ⁻¹	1.360	1.345	1.115%	1.317	3.265%
Core inlet temperature/K	1144.0	1144.0	0%	1144.44	0%
Turbine outlet temperature/K	970.976	960	1.143%	960	0.23%
Outlet temperature of the hot end of the recuperator/K	556.137	557.6	0.262%	557.6	0.262%
compressor inlet temperature/K	403.0	403.0	0%	/	/
compressor outlet temperature/K	524.812	528	0.604%	/	/
Pile inlet temperature/K	939.651	938.5	0.123%	944.172	0.479%
System power generation/MW	0.0298	0.0301	0.997%	/	/

Table 2. Comparison of simulated and reference values

382 radioactivity, but it takes up too much space and has addi-
 383 tional power consumption. The direct and indirect Brayton
 384 cycle circuits with 40g/mol of helium-xenon gas mixture as
 385 the flow medium are simulated by EBSILON with the same
 386 thermal power of 3MW. The main pump of the first circuit of
 387 the indirect Brayton cycle is replaced by a compressor, and
 388 the numerical transmitter is used to control the same flow
 389 rate of the first and second circuits. The simulation results
 390 are shown in Fig 6: At this time, three parameters, namely
 392 turbine inlet temperature, pressure ratio and compressor inlet
 393 temperature, were varied to observe the change of the effi-
 394 ciency of the direct and indirect Brayton cycles at different
 396 parameters. The results are shown in Fig 7: The results show
 397 that the direct and indirect Brayton cycles follow the same
 398 trend as each system parameter changes. However, the ef-
 399 ficiency of the direct Brayton cycle is 1.4% to 2.8% higher
 400 than that of the indirect Brayton cycle. This is because, on
 401 the one hand, the system components of the indirect Brayton
 402 cycle are more than those of the direct Brayton cycle, which
 403 leads to an increase in the pressure loss of the system. On
 404 the other hand, the first circuit of the indirect Brayton cycle
 405 contains one more pump, which acts as a power-consuming
 406 component. So the power dissipation of the system increases,
 407 which leads to a decrease in efficiency. Therefore, in practi-
 408 cal applications for high-power missions such as deep space
 409 exploration, the direct Brayton cycle is more suitable. It has
 410 higher efficiency in a more compact structure[26]. Although
 411 the indirect Brayton cycle is able to isolate radioactivity in
 412 the reactor primary loop, such an advantage is not obvious in
 413 specific contexts.

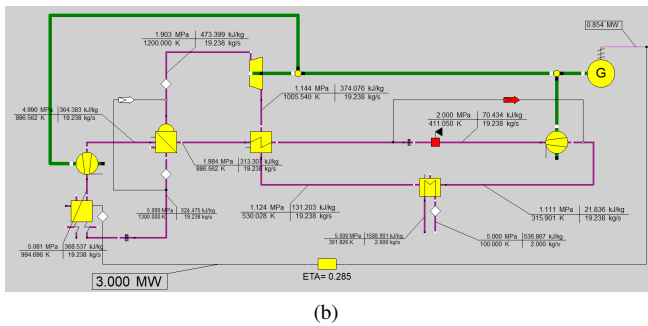
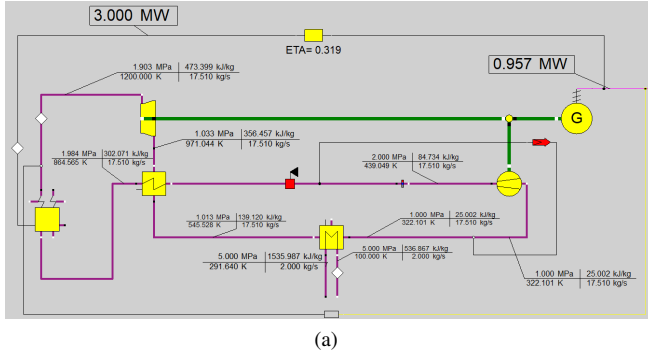
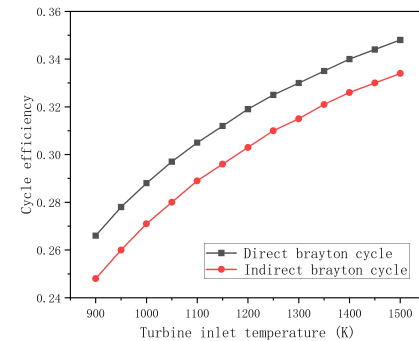
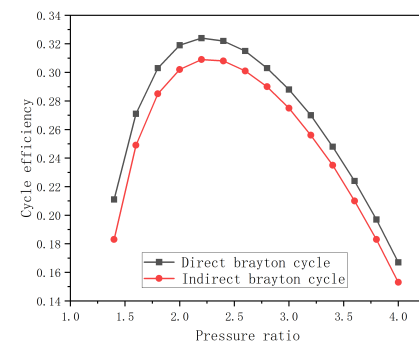


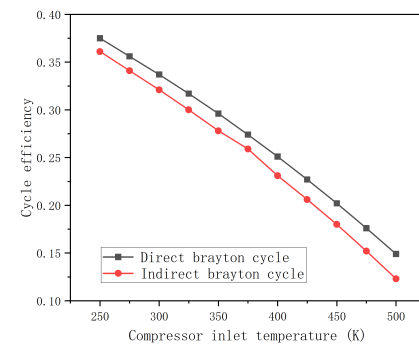
Fig. 6. The simulation of direct and indirect Brayton cycle in EBSILON



(a)



(b)



(c)

Fig. 7. The cycle efficiency comparison of the direct and indirect Brayton cycle

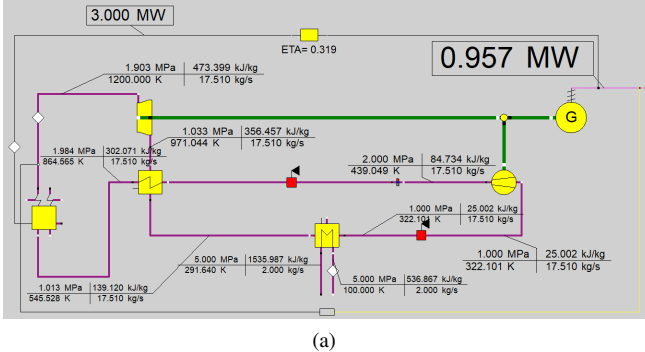
414
415

B. Comparison of the efficiency of four Brayton cycle structures

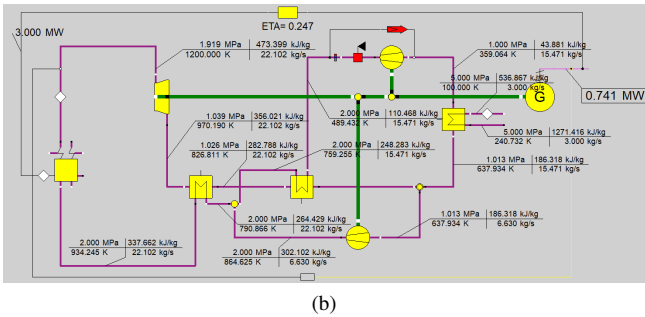
416 For the Brayton cycle, in order to increase its efficiency,
417 researchers improve its structure by adding interstage-cooled
418 and recompression, among other things. For gases such as
419 air and supercritical CO₂, recompression cycle is generally
420 used[27–29]. For helium-xenon gas mixtures which has high
421 adiabatic index, the applicability of different Brayton cy-
422 cle structures may be different from other types of gases.
423 The four Brayton cycle structures are modeled and simu-
424 lated using EBSILON, as shown in Fig 8: In EBSILON,
425 both the compressor inlet temperature and the turbine inlet
426 temperature can be used as boundary conditions to design
427 the complete circuit. Therefore, the effect of turbine inlet
428 temperature on the efficiency of different Brayton structures
429 is investigated. And then the efficiency of different Bray-
430 ton cycle structures is observed and compared. The com-
431 pressor inlet temperatures are selected of 300K, 350K and
432 400K, and the turbine inlet temperature varies from 950K
433 to 1500K. The simulation results are shown in Fig 9: As
434 shown in Fig 9 (a), $\eta_{interstage-cooled} > \eta_{simple reheat} >$
435 $\eta_{interstage-cooled recompression} > \eta_{recompression}$ at compres-
436 sor inlet temperature of 400K. When the turbine inlet tem-
437 perature is 1000K, the recompression cycle efficiency is only
438 9.1%. And when the turbine inlet temperature is lower than
439 1200K, the recompression cycle efficiency is lower than 20%.
440 It is due to the large adiabatic index of the helium-xenon mix-
441 ture (stable at high temperatures around 1.67), which makes
442 the effect of compressor power dissipation larger. When the

443 turbine inlet temperature is higher than 1400K, the efficiency
444 of both interstage-cooled cycle and simple reheat cycle is
445 higher than 30%. The difference in efficiency between the
446 two is less than 2%. Considering the compactness of the
447 structure, the simple reheat cycle is a better structure.

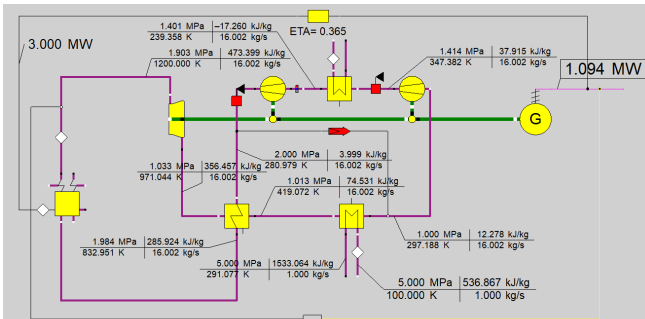
448 As shown in Fig 9 (b), when the turbine inlet tem-
449 perature is 1200K and 1500K, the simple reheat cy-
450 cle efficiency is 29.6% and 35.2%, respectively. And
451 when the turbine inlet temperature is less than 1350K,



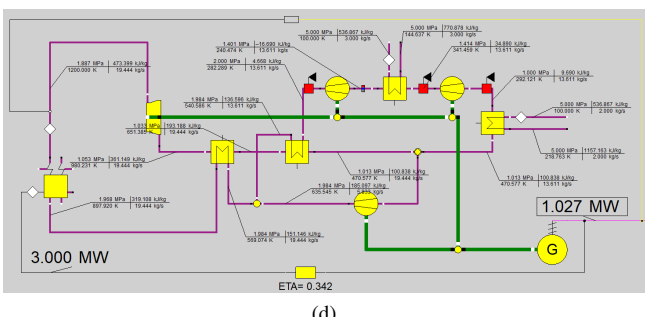
(a)



(b)

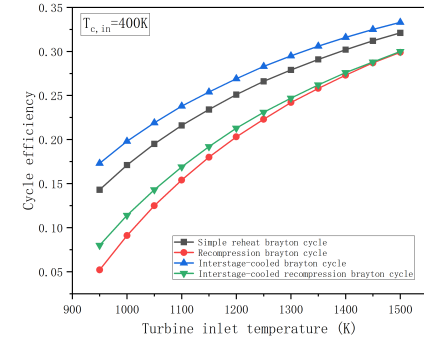


(c)

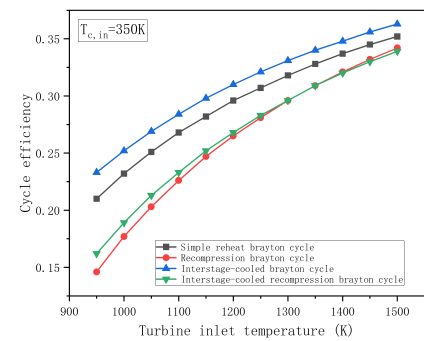


(d)

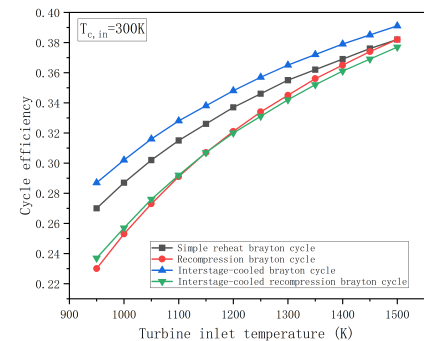
Fig. 8. The simulation of four structures of Brayton cycle using EBSILON



(a)



(b)



(c)

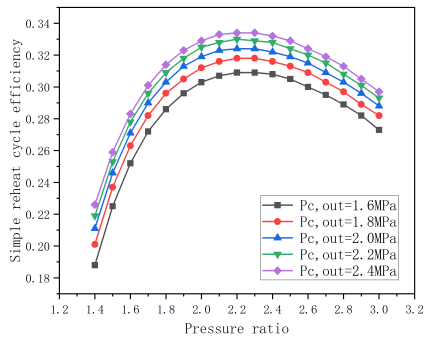
Fig. 9. The simulation results of different Brayton cycle structures

higher than 30%. Besides, the efficiency of both the recompression cycle and the simple reheat cycle is 38.2% when the turbine inlet temperature reaches 1500K. This is due to the fact that at low compressor inlet temperatures, the additional power dissipation due to the recompressor is low, and the negative effect on the cycle efficiency is close to the positive effect due to the reactor inlet enthalpy increase.

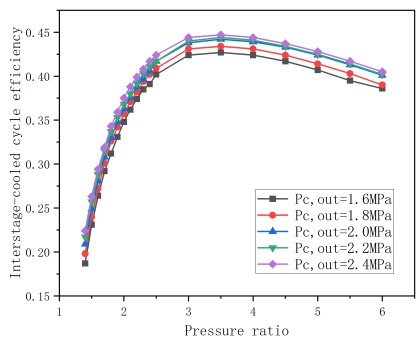
In the actual study, considering the physical properties of the work material, the material properties of the components and the cost, it is difficult to further increase the turbine inlet

454 $\eta_{\text{interstage-cooledrecompression}} > \eta_{\text{recompression}}$. When
455 the turbine inlet temperature is more than 1350K,
456 $\eta_{\text{interstage-cooledrecompression}} < \eta_{\text{recompression}}$.

457 As shown in Fig 9 (c), when the compressor inlet tem-
458 perature is 300K, the efficiency of all four cycle struc-
459 tures is higher than 20%. And when the turbine inlet tem-
460 perature is higher than 1150K, the efficiency of all four structures is

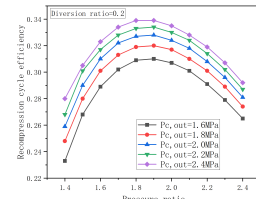


(a)

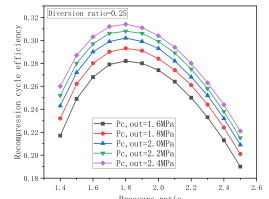


(b)

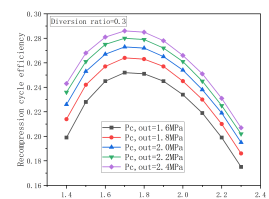
Fig. 10. The effect of the pressure ratio on the Brayton cycle efficiency



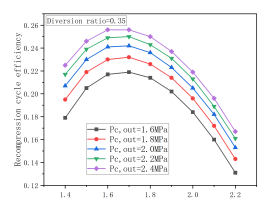
(a)



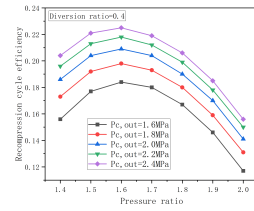
(b)



(c)



(d)



(e)

Fig. 11. The effect of the pressure ratio on the recompression Brayton cycle efficiency with different diversion ratios

temperature and further reduce the compressor inlet temperature. Therefore, summarizing the above results, The simple reheat cycle has a large advantage regardless of changes in compressor and turbine inlet temperatures.

C. Effect of pressure ratio on efficiency

In the Brayton cycle loop, the maximum and minimum pressure are located at the inlet and outlet of the compressor, and the ratio of the two is called the pressure ratio. In this study, by controlling the compressor outlet pressure to a constant value (1.6MPa, 1.8MPa, 2.0MPa, 2.2MPa, 2.4MPa), the pressure ratio is changed to investigate the effect on the efficiency. The simulation results of simple reheat cycle and interstage-cooled cycle are shown in Fig 10:

For the simple reheat cycle, when the compressor outlet pressure is different, the curves of the cycle efficiency satisfy the trend of increasing and then decreasing, and all of them get the maximum value at the pressure ratio of 2.2. At a pressure ratio of 2.2, the cycle efficiency increases from 30.9% to 33.4% as the compressor outlet pressure increases from 1.6MPa to 2.4MPa. As for the interstage-cooled cycle, the efficiency is more sensitive to the change of pressure ratio

before the efficiency obtains the maximum value. And after the efficiency obtains the maximum value, the efficiency changes with the pressure ratio more slowly. Regardless of the value of the compressor outlet pressure, the pressure ratio at which the system's circulation efficiency is maximized is 3.5. And the cycle efficiency increased from 42.7% to 44.7% as the compressor outlet pressure increased from 1.6 MPa to 2.4 MPa.

In addition, the simulation studies on the optimum pressure ratio of the recompression cycle are carried out with the diversion ratios of 0.2, 0.25, 0.3, 0.35, and 0.4, respectively, and the results are shown in Fig 11. The results show that the optimal pressure ratios of the recompression cycles are different at different diversion ratios. The larger the diversion ratio, the smaller the corresponding optimal pressure ratio. The recompression cycle with the optimal pressure ratio achieves the maximum cycle efficiency when the split ratio is 0.2 and the compressor outlet pressure is 2.4 MPa. At this time, the cycle efficiency is 0.339, which is approximately equal to the maximum efficiency of the simple reheat cycle and much smaller than the maximum efficiency of the interstage-cooled cycle.

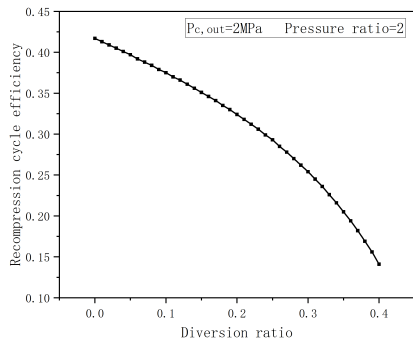


Fig. 12. The effect of the diversion ratio on the recompression Brayton cycle efficiency

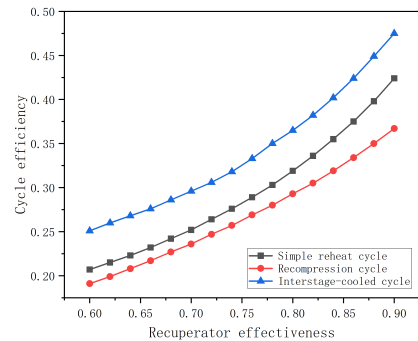


Fig. 13. The influence of the recuperator effectiveness on the cycle efficiency

515 D. Effect of diverter ratio on recompression efficiency

516 The above results show that the diversion ratio has an effect
 517 on the recompression cycle efficiency. Therefore, the diver-
 518 sion ratio of the splitter is changed to observe the change of
 519 the cycle efficiency.. Since the results described in the previ-
 520 ous section show that the recompression cycle efficiency has
 521 reached a very low level when the pressure ratio is taken as
 522 2.0 and the shunt ratio is 0.4. Therefore, the diversion ra-
 523 dio is changed from 0 to 0.4 to obtain the results shown in
 524 Fig 12: When the diversion ratio increases from 0 to 0.4, the
 525 efficiency of the recompression cycle decreases, and the mag-
 526 nitude of change is large. Obviously, when the recompression
 527 diversion ratio is close to 0, the recompressor does not con-
 528 sume power, and the recompression cycle is infinitely close
 529 to the simple recuperation cycle with two recuperators. Ac-
 530 cording to the results of the previous study, the simple reheat
 531 cycle efficiency is higher than the recompression cycle, and
 532 contains two recuperators, so the cycle efficiency can be in-
 533 creased to 41.7%. And when the diversion ratio tends to 1,
 534 the system tends to Brayton cycle without recuperators, the
 535 cycle efficiency is greatly reduced. When the diversion ratio
 536 is 0.4, the cycle efficiency is only 14.1%.

538 E. Influence of recuperator on efficiency

539 On the basis of the above simulation results, the influence
 540 of the recuperator effectiveness on the efficiency of Bray-
 541 ton cycle is investigated, and the results are shown in Fig
 542 13: It is easy to find that, regardless of the structure of the
 543 Brayton cycle, increasing the recuperator effectiveness can
 544 effectively improve the cycle efficiency of the system. When
 545 the recuperator effectiveness is increased from 0.6 to 0.9, the
 546 simple reheat cycle efficiency is increased by 21.7%. More-
 547 over, when the recuperator effectiveness reaches 0.78, the ef-
 548 ficiency of simple reheat cycle can be higher than 30%. For
 549 the interstage-cooled cycle, its efficiency is always about 5%
 550 higher than that of the simple reheat cycle. However, the
 551 simple reheat cycle has greater applicability to the interstage-

553 cooled cycle because it has one more cooler than interstage-
 554 cooled cycle.

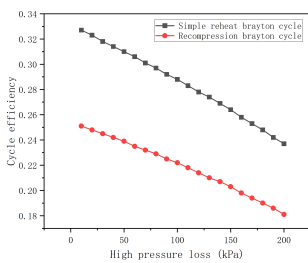
555 F. Effect of pressure loss on efficiency

556 In the Brayton cycle circuit, pressure loss is inevitable, in-
 557 cluding pressure loss of the cooler, recuperators and other
 558 components, as well as the pressure loss of the pipeline. The
 559 pipeline pressure loss was divided into high pressure loss and
 560 low pressure loss, and the high pressure and low pressure loss
 561 were defined in EBSILON by setting the pipeline at the inlet
 562 and outlet of the compressor, so as to study the effect of the
 563 two on the cycle efficiency of the system respectively. The
 564 results of the study are shown in Fig 14.

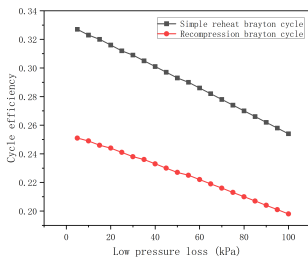
565 The results showed that when the high pressure relative
 566 pressure loss was increased from 0% to 10%,the efficiency
 567 of simple reheat cycle and recompression cycle decreased by
 568 9% and 7%, respectively. Whereas, when the relative low
 569 pressure loss was increased from 0% to 10%, the efficiency
 570 of both decreased by 7.3% and 5.3%, respectively. The effect
 571 of the high pressure relative pressure loss on the cycle effi-
 572 ciency is slightly higher than that of the low pressure relative
 573 pressure loss, this is because the effect of the high pressure
 574 relative loss on the pressure ratio is higher.

576 G. Impact of TAC on efficiency

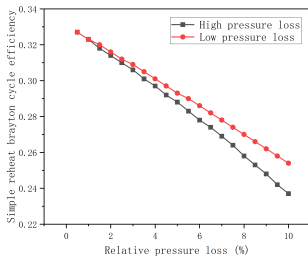
577 The efficiencies of the turbine, compressor and generator
 578 all affect the efficiency of the Brayton cycle, and the effi-
 579 ciencies of the turbine and compressor include isentropic and
 580 mechanical efficiencies. The change of the cycle efficiency
 581 with different mechanical efficiency is studied by setting the
 582 isentropic efficiencies of 0.80, 0.82, 0.84, 0.86, 0.88 and 0.90
 583 for the turbine and compressor. And the effect of the gen-
 584 erator efficiency on the cycle efficiency is also carried out.
 585 The simulation results are shown in Fig 15. It is easy to see
 586 that increasing the efficiency always increases the system cy-
 587 cle efficiency, regardless of the component. For the turbine,



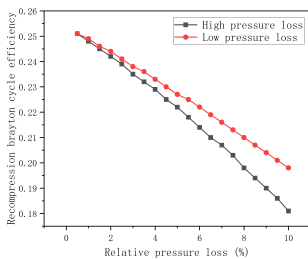
(a)



(b)



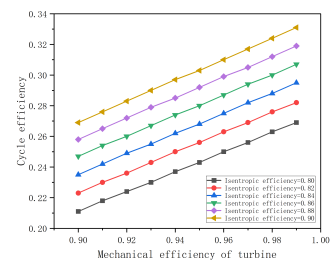
(c)



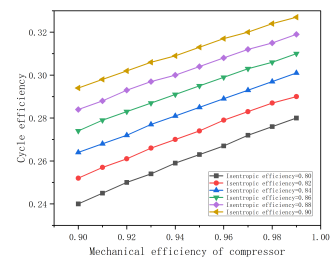
(d)

Fig. 14. The effect of the high and low pressure loss on the cycle efficiency

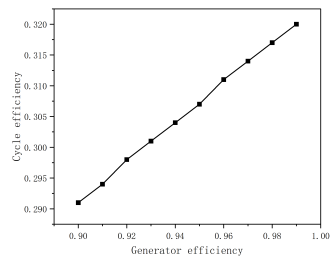
increasing its mechanical efficiency at a certain isentropic efficiency increases the system cycle efficiency by about 6%. And increasing its isentropic efficiency at a certain mechanical efficiency increases the system efficiency by about 5%. For the compressor, the two values are 3.5% and 5%, respectively. And when the generator efficiency is increased from 0.9 to 0.99, the system efficiency increases by 2.9%.



(a)



(b)



(c)

Fig. 15. The effect of the TAC on the cycle efficiency

596

H. Exergy analysis

In thermodynamics, exergy is an important parameter. For a cycle loop, analyzing the magnitude and distribution of the energy loss is essential to evaluate its economy and thermal efficiency. Based on the first and second laws of thermodynamics, the method of performance analysis can elucidate the transformations, transfers, utilization, and losses of exergy, and ultimately quantify the performance efficiency of a system or equipment[30].

The method of exergy analysis was used to calculate and analyze the exergy utilization efficiency of Simple reheat cycle and Recompression cycle. And the EBSILON is used to obtain the distribution of the energy loss of the two and to analyze the reasons for the low efficiency of the cycle. And provide guidance for the improvement of their cycle efficiency. The calculated results of the exergy of each component of Simple reheat cycle (1200 K, 2 MPa) are shown in Table 3, Fig. 16 and Fig 17:

		Unit	Turbine inlet	Turbine outlet	Shaft power	
Turbine	Mass flow rate	kg/s	17.510	17.510	/	
	Exergy	kJ/kg	430.593	309.092	2027	
	Exergy loss	kJ/kg		100.483		
	Input	kJ/kg		2127.483		
	Exergy efficiency	%		95.277		
Recuperator	Unit	Hot end inlet of the recuperator	Hot end outlet of the recuperator	Cold end inlet of the recuperator	Cold end outlet of the recuperator	
	Mass flow rate	kg/s	17.510	17.510	17.510	
	Exergy	kJ/kg	309.092	179.307	184.981	307.332
	Exergy loss	kJ/kg		273.681		
	Input	kJ/kg		2416.047		
Cooler	Exergy efficiency	%		88.672		
	Unit	Hot end inlet of the cooler	Hot end outlet of the cooler	Cold end inlet of the cooler	Cold end outlet of the cooler	
	Mass flow rate	kg/s	17.510	17.510	2.000	2.000
	Exergy	kJ/kg	179.307	132.529	2289.337	2343.222
	Exergy loss	kJ/kg		583.930		
Compressor	Input	kJ/kg		838.636		
	Exergy efficiency	%		30.371		
	Unit	Compressor inlet	Compressor outlet	Consumed power		
	Mass flow rate	kg/s	17.510	17.510	/	
	Exergy	kJ/kg	132.529	184.981	1056	
Reactor	Exergy loss	kJ/kg		89.448		
	Input	kJ/kg		1056		
	Exergy efficiency	%		91.530		
	Unit	Reactor inlet	Reactor outlet	Power input		
	Mass flow rate	kg/s	17.510	17.510	/	
Reactor	Exergy	kJ/kg	307.332	430.593	3000	
	Exergy loss	kJ/kg		841.700		
	Input	kJ/kg		3000		
	Exergy efficiency	%		71.943		

Table 3. Calculation of the exergy of each part of the Simple reheat cycle

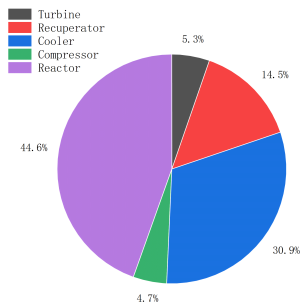


Fig. 16. Proportion of exergy loss in each part of Simple reheat cycle

In Simple reheat cycle, the reactor and external cooler have higher losses, accounting for 44.6% and 30.9% of the total, respectively. The losses in the turbine and compressor are smaller, 5.3% and 4.7%, respectively. The reactor and external cooler also have lower exergy efficiencies, while the latter is only 30.371%, which is one of the major reasons for the lower system efficiency. The calculated results of the densities of the components of the recompression cycle (1200 K, 2 MPa) are shown in Table 4, Fig 18 and Fig 19: As in Simple reheat cycle, the losses in the recompression cycle are concentrated in the reactor and external cooler, which have losses of 37.6% and 42.0%, respectively. The remaining components have relatively small losses. The external cooler of the reactor has a lower energy efficiency, while the energy

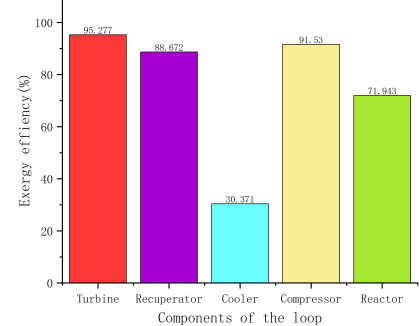


Fig. 17. Exergy efficiency of the main equipment of simple reheat cycle

		Unit	Turbine inlet	Turbine outlet	Shaft power	
Turbine	Mass flow rate	kg/s	22.102	22.102	/	
	Exergy	kJ/kg	431.061	309.102	2568	
	Exergy loss	kJ/kg			127.538	
	Input	kJ/kg			2695.538	
	Exergy efficiency	%			95.269	
Recuperator 1	Unit	Hot end inlet of the recuperator	Hot end outlet of the recuperator	Cold end inlet of the recuperator	Cold end outlet of the recuperator	
	Mass flow rate	kg/s	22.102	22.102	22.102	22.102
	Exergy	kJ/kg	309.102	257.478	282.569	332.557
	Exergy loss	kJ/kg			36.159	
	Input	kJ/kg			1140.994	
Recuperator 2	Exergy efficiency	%			96.831	
	Unit	Hot end inlet of the recuperator	Hot end outlet of the recuperator	Cold end inlet of the recuperator	Cold end outlet of the recuperator	
	Mass flow rate	kg/s	22.102	22.102	15.471	15.471
	Exergy	kJ/kg	257.478	207.511	195.558	272.114
	Exergy loss	kJ/kg			163.846	
Cooler	Input	kJ/kg			1348.244	
	Exergy efficiency	%			87.847	
	Unit	Hot end inlet of the cooler	Hot end outlet of the cooler	Cold end inlet of the cooler	Cold end outlet of the cooler	
	Mass flow rate	kg/s	15.471	15.471	2.000	2.000
	Exergy	kJ/kg	207.511	137.780	2289.337	2384.808
Compressor	Exergy loss	kJ/kg			919.594	
	Input	kJ/kg			1110.536	
	Exergy efficiency	%			17.194	
	Unit	Compressor inlet	Compressor outlet	Consumed power		
	Mass flow rate	kg/s	15.471	15.471	/	
Recompressor	Exergy	kJ/kg	137.780	195.558	1041	
	Exergy loss	kJ/kg			80.963	
	Input	kJ/kg			1041	
	Exergy efficiency	%			92.223	
	Unit	Recompressor inlet	Recompressor outlet	Consumed power		
Reactor	Mass flow rate	kg/s	6.630	6.630	/	
	Exergy	kJ/kg	207.511	307.802	775	
	Exergy loss	kJ/kg			36.915	
	Input	kJ/kg			775	
	Exergy efficiency	%			95.237	
Reactor	Unit	Reactor inlet	Reactor outlet	Power input		
	Mass flow rate	kg/s	22.102	22.102	/	
	Exergy	kJ/kg	332.557	431.061	3000	
	Exergy loss	kJ/kg			822.865	
	Input	kJ/kg			3000	
	Exergy efficiency	%			72.571	

Table 4. Calculation of the exergy of each part of Recompression cycle

efficiency of the external cooler is only 17.194%, which is the direct reason for the lower recompression efficiency.

Based on the above study, it can be seen that the efficiency

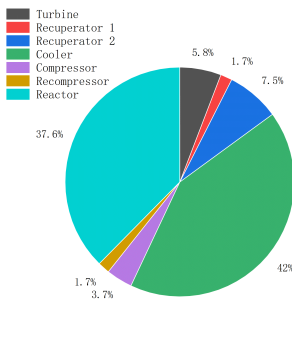


Fig. 18. Proportion of exergy loss in each part of Recompression cycle

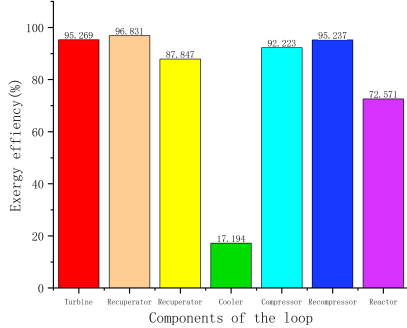


Fig. 19. Exergy efficiency of the main equipment of simple reheated cycle

of the recompression cycle is lower than that of simple reheat cycle in most cases. By means of the method of exergy analysis, a comparative plot of the energy loss between the two was obtained, as shown in Fig 20: With the exception of the recuperator and the reactor, the recompression cycle has higher losses than the simple reheat cycle. Especially for the external cooler, the loss of the recompression cycle is 919.594 kJ/kg, which is much larger than that of the simple reheat cycle, which is 583.93 kJ/kg. Although the recompression cycle increases the inlet enthalpy of the reactor, the irreversible loss carried away by the external cooler source is much more. And it leads to the reduction of the net system work, and therefore results in the reduction of the system efficiency.

In summary, a simple reheat cycle loop with 3 MW of thermal power and 1 MW of electrical power is designed using EBSILON. The parameters of the system are shown in the Table 4. The system is able to fulfill the space exploration missions at the MW power level and maintains a high loop efficiency while considering a relative pressure loss of 5%. The system schematic is shown in Fig 21.

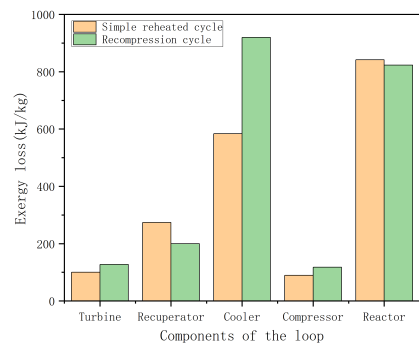


Fig. 20. The exergy loss comparison of Simple reheat cycle and Recompression cycle

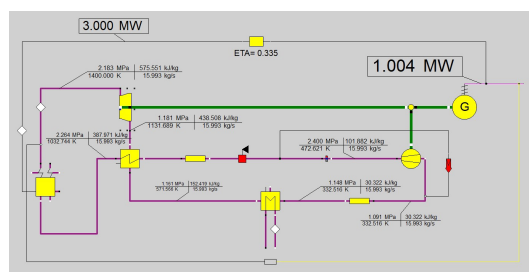


Fig. 21. The system designed in EBSILON

Parameter	Value	Parameter	Value
Thermal power/MWt	3	cyclic efficiency	0.335
Electric power/MWt	1.004	Recuperator effectiveness	0.85
Coolant flow/kg · s ⁻¹	15.993	Turbomachinery efficiency	0.99
Turbine inlet temperature/K	1400	Turbine isentropic efficiency	0.88
Inlet temperature of the hot end of the recuperator/K	1131.689	Mechanical efficiency of pressurized air	0.99
Cooler inlet temperature/K	571.566	Isentropic efficiency of a pressurized gas engine	0.88
Compressor inlet temperature/K	332.516	Generator efficiency	0.99
Cold end inlet temperature of recuperator/K	472.621	Maximum cycle pressure/MPa	2.4
Pile inlet temperature/K	1032.744	pressure ratio	2.2

Table 5. The parameters of the system designed

IV. CONCLUSION

In this paper, the Brayton cycle of a gas-cooled reactor with a thermal power of 3 MW is taken as a research object to study the efficiency comparison of Brayton cycles with different structures as well as the sensitivity analysis, and the main conclusions are as follows:

(1) For the direct and indirect Brayton cycle loops, the efficiency comparison between the two is carried out by vary-

ing the inlet temperatures and pressure ratios of the turbine and the compressor and the rest of the boundary conditions is controlled to be the same. It was found that direct cycle is 1.4% to 2.8% more efficient than indirect cycle.

(2) For four common Brayton cycle configurations, the efficiencies of the four configurations were compared by varying the turbine inlet temperature while controlling for a certain compressor inlet temperature. It is shown that at higher compressor inlet temperatures, recompression cycle negatively affects the efficiency, while the interstage-cooled Brayton cycle and simple reheat cycle have the highest efficiency. The efficiency of both is higher than 30% at turbine inlet temperatures above 1400K. At slightly higher compressor inlet temperatures, the interstage-cooled and simple reheat cycles still have high efficiencies, and when the turbine inlet temperature is less than 1350K, $\eta_{interstage-cooledrecompression} > \eta_{recompression}$, when the turbine inlet temperature is higher than 1350K, $\eta_{interstage-cooledrecompression} < \eta_{recompression}$. At lower compressor inlet temperatures, the efficiency of all four cycles is higher than 20%. At a turbine inlet temperature of 1500K, the efficiency of both the recompression cycle and the simple reheat cycle is 38.2%. The negative effect from the recompressor disappears.

(3) The pressure ratio also has a large effect on the efficiency of the Brayton cycle. For the simple reheat cycle and the interstage cooling cycle, the optimal pressure ratios are

2.2 and 3.5, respectively, and the magnitude of the optimal pressure ratio is independent of the maximum system pressure. For the recompression cycle that needs to consider the split ratio, it is shown that different split ratios correspond to different optimal pressure ratios, and the larger the split ratio is, the smaller the corresponding optimal pressure ratio is;

(4) The diversion ratio has a large effect on the efficiency of the recompression cycle, which decreases as the diversion ratio increases. When the diversion ratio increases from 0 to 0.4, the circulation efficiency decreases from 0.417 to 0.141. This is due to the fact that a low diversion ratio converges to a simple reheat cycle with two recuperators, while a high diversion ratio converges to a Brayton cycle without recuperators. In addition, the number of recuperators and the regenerator effectiveness also have an effect on the efficiency of the Brayton cycle;

(5) By setting the relative pressure loss between the inlet and outlet of the compressor to simulate the pressure loss in the actual working condition, it is found that the high pressure loss has a slightly larger effect. The efficiency of simple reheat cycle and recompression cycle are reduced by 9% and 7% respectively when the high pressure relative loss increases from 0% to 10%.

(6) The efficiency of the TAC components will affect the cycle efficiency to some extent and can be maximized in practical engineering.

- [1] H.P. Mei, D.L. Yu, S.Q. Ma et al. Conceptual design for a 5 kWe space nuclear reactor power system[J].NUCLEAR ENGINEERING AND TECHNOLOGY,2024,56,(9):3644-3653.
- [2] P. Liu, J. Tian, P. Sun et al. Cascade control system design for a space nuclear reactor[J].ANN NUCL ENERGY,2024,208110760-110760. DOI:10.1016/J.ANUCENE.2024.110760.
- [3] Koroteev AS, Akimov VN, Popov SA. Project of creation of transport-power module on the basis of nuclear power propulsion system of megawatt type[J]. Poliot Mag, 2011, 4: 93-99.
- [4] Blott R, Koppel C, Valentian D, et al. Disruptive Technologies for Power and Propulsion (DiPoP) Fission Nuclear Options[C]. 64th International Astronautical Congress. 2013.
- [5] JANSEN F, BAUER W, MASSON F, et al. DEMOCRITOS Demonstrators for Realization of Nuclear Electric Propulsion of the European Roadmaps MEGAHit&DiPoP[J].T JPN SOC AERONAUT S, AEROSPACE TECHNOLOGY JAPAN, 2016,14(ists30):Pb_225-Pb_233. DOI:10.2322/TASTJ.14.PB_225.
- [6] W.X. Ju, K.W. Ning, F.L. Zhao et al. Modelling Research and Performance Analysis on a Megawatt-Level Helium-Xenon Gas Cooled Small Reactor Based on the Thermal-Hydraulic Constraints[J].SSRN,2024,DOI:10.2139/ssrn.4885295.
- [7] X. Yang, D. She, L. Shi. Neutronics Analysis of Small Compact Prismatic Nuclear Reactors for Space Crafts[J].JOURNAL OF NUCLEAR ENGINEERING AND RADIATION SCIENCE,2018,4,(2):021006.DOI:10.1115/1.4038774.
- [8] B.H. Jiang, Y. Ji , J. Sun et al. Shielding mass estimation model for gas-cooled space nuclear reactors[J].NUCL ENG DES,2024,424,DOI:10.1016/j.nucengdes.2024.113238.
- [9] K. Yue, C.L. Wang, R. Zhang et al. Shutdown safety analysis of megawatt-class space gas-cooled reactor system[J].PROG NUCL ENERG,2023,161,DOI:10.1016/j.pnucene.2023.104727.
- [10] H. Qin, C.L. Wang, W.X. Tian et al. Energy allocation optimization of the gas-cooled space nuclear reactor[J].APPL THERM ENG,2021,196,DOI:10.1016/j.applthermaleng.2021.117289.
- [11] T. Meng, K. Cheng, F. Zhao et al. Computational flow and heat transfer design and analysis for 1/12 gas-cooled space nuclear reactor[J].ANN NUCL ENERGY,2020,135106986-106986.DOI:10.1016/j.anucene.2019.106986.
- [12] Z. Li, J. Sun, M. Liu et al. Design of a hundred-kilowatt level integrated gas-cooled space nuclear reactor for deep space application[J].NUCL ENG DES,2020,361(prepublis):110569-110569. DOI:10.1016/j.nucengdes.2020.110569.
- [13] Biondi, Alfonso,Toro, Claudia. Closed Brayton Cycles for Power Generation in Space:Modeling,simulation and exergy analysis[J].ENERGY,2019,181, 793-802.
- [14] Ribeiro Guilherme B, Braz Filho Francisco A, Guimaraes Lamartine N. F. Thermodynamic analysis and optimization of a Closed Regenerative Brayton Cycle for nuclear space power systems[J].APPLIED THERMAL ENGINEERING,2015,90,250-257.
- [15] Y. Wu, S. Tang, L. Zhu, et al.Transient analysis of megawatt-level space gas-cooled reactor coupled with He-Xe Brayton cycle system[J].APPL THERM ENG,2025,260124962-124962.DOI:10.1016/J.APPLTHERMALENG.2024.124962
- [16] Xianbo W, Xianmin D, Zhongchun L, et al. Transient characteristics analysis of residual heat removal system for Helium-Xenon mixture cooled small reactor system[J].NUCL ENG DES,2024,424,DOI:10.1016/j.nucengdes.2024.113238.

- 779 DES,2023,410.DOI:10.1016/J.NUCENGDES.2023.112387.
- 780 [17] Malik A, Zheng Q, Lin A. The design and performance
781 analysis of highly loaded compressor of closed Brayton cy-
782 cle HTGR power plant with helium-xenon gas mixture as
783 working fluid[J].Progress in Nuclear Energy,2019,117103084-
784 103084. DOI:10.1016/j.pnucene.2019.103084.
- 785 [18] W.K. Ma, P. Ye, G. Zhao et al. Effect of cool-
786 ing schemes on performance of MW-class space
787 nuclear closed Brayton cycle[J].ANN NUCL EN-
788 ERGY2021,162,DOI:10.1016/j.anucene.2021.108485.
- 789 [19] C.L. Wang, S.Y. C, W.X. Tian et al. Thermal-hydraulic anal-
790 ysis of He-Xe gas mixture in 2×2 rod bundle wrapped with
791 helical wires[J].NUCL ENG TECHNOL,2023,55(7):2534-
792 2546.DOI:10.1016/J.NET.2023.04.013.
- 793 [20] King JC, El-Genk MS. Thermal-hydraulic and neutronic anal-
794 yses of the submersion-subcritical, safe space (S^4) reactor[J].
795 NUCL ENG DES, 2009, 239(12): 2809-2819.
- 796 [21] B. Jiang, Y. Ji, J. Sun et al. Dynamic analysis
797 code development for space nuclear power sys-
798 tems[J].PROG NUCL ENERG,2025,180105601-105601.
799 DOI:10.1016/J.PNUCENE.2024.105601.
- 800 [22] Koroteev AS, Akimov VN, Popov SA. Project of creation of
801 transport-power module on the basis of nuclear power propul-
802 sion system of megawatt type[J].Poliot Mag, 2011, 4: 93-99.
- 803 [23] Wright SA, Lipinski RJ, Vernon ME, et al. Closed Brayton cy-
804 cle power conversion systems for nuclear reactors: modeling,
805 operations, and validation[J]. Sandia Rep, 2006: 1-257.
- 806 [24] HIRSCHFELDER J O, CURTISS C F,BIRDR. Molecular
807 theory of gases and fluids[M].New York:John Wiley and Sons,1954.
- 808 [25] A. Zhang, X. Wang. Development of Modelica-based one-
809 dimensional thermodynamic cycle library and its applica-
810 tion in simulation and multi-objective optimization of a
811 He-Xe closed-Brayton-cycle system[J].PROG NUCL EN-
812 ERG,2024,172,DOI:10.1016/j.pnucene.2024.105205.
- 813 [26] W. Ma, X. Yang, J. Wang. Power regulation methods and reg-
814 ulation characteristics of the space reactor direct Brayton cycle
815 with helium-xenon working fluid[J].Energy,2024,313134012-
816 134012. DOI:10.1016/J.ENERGY.2024.134012.
- 817 [27] G.Y. Peng, Y.C. Peng, Z. Na, et al. Multi-objective
818 optimization and evaluation of supercritical CO₂ Bray-
819 ton cycle for nuclear power generation[J].NUCL SCI
820 TECH,2024,35(2).DOI:10.1007/S41365-024-01363-Y.
- 821 [28] Ahn Y, Lee J, Kim G S, et al. Design consid-
822 eration of supercritical CO₂ power cycle inte-
823 gral experiment loop[J].Energy,2015,86115-127.
824 DOI:10.1016/j.energy.2015.03.066
- 825 [29] Park H J, Park S H, Kwon G J, et al. Optimiza-
826 tion and thermodynamic analysis of supercriti-
827 cal CO₂ Brayton recompression cycle for various
828 small modular reactors[J].Energy,2018,160520-535.
829 DOI:10.1016/j.energy.2018.06.155.
- 830 [30] H. Hu, Y. Jiang, C. Guo, et al. Thermodynamic and ex-
831 ergy analysis of a S-CO₂ Brayton cycle with various of
832 cooling modes[J].ENERG CONVERS MANAGE,2020,220.
833 DOI:10.1016/j.enconman.2020.113110.
- 834